

## Supplementary Information

### 0.1 Dataset and model setup

The training dataset contains a diverse set of gold clusters ranging from 10 to 140 atoms, including compact, planar, and cage structures. The DFT reference energies were computed with the Projector-Augmented Wave (PAW) method [1, 2] using 11 valence electrons as implemented in the Vienna Ab initio Simulation Package (VASP) [3, 4] together with the PBE exchange-correlation functional [5]. To remove interactions between periodic images, a vacuum of 12 Å was introduced in all directions around the nanoclusters. Figures S1 and S2 show the distribution of cluster sizes and total energies in the training set, respectively.

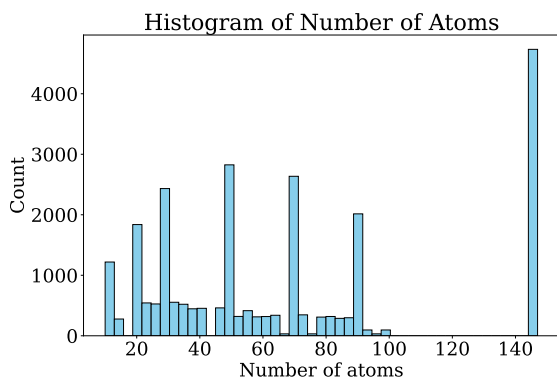


Fig. S1: Histogram of the number of atoms in the training dataset.

The NequIP model was trained for 82 epochs using a force-matching loss that combines force and energy contributions. The network architecture, radial cutoff, number of interaction blocks, and angular-momentum channels were chosen to balance accuracy and computational efficiency.

### 0.2 Performance and application

The final NequIP model reproduces the DFT reference data with high accuracy for both energies and forces and is therefore suitable as a surrogate po-

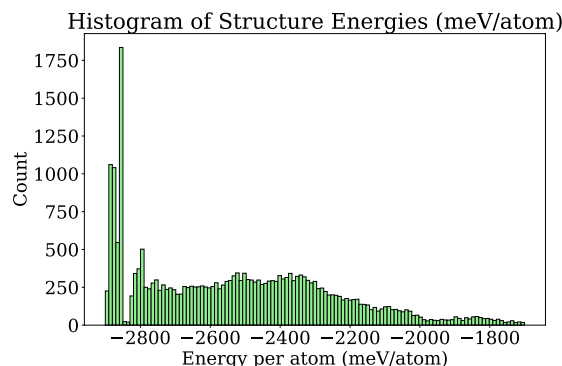


Fig. S2: Energy distribution of structures in the training dataset (meV/atom).

tential for global structure searches. Detailed performance metrics, including root-mean-square errors (RMSEs) for energies and forces on the training and validation sets, are summarized in table SI. A comparison with other interaction models is shown in fig. S3.

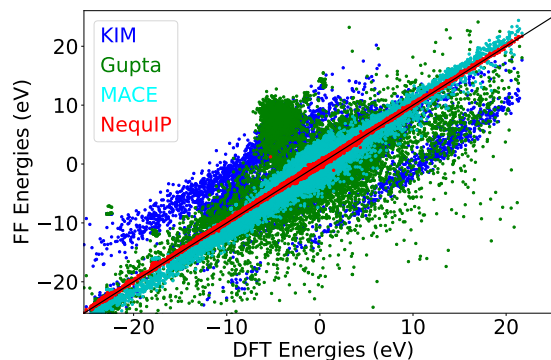


Fig. S3: Correlation of total energies by EAM method [6, 7], Gupta [8], MACE and NequIP models with DFT reference energies for a representative set of gold cluster configurations.

### 0.3 Validation of the charge-corrected NequIP potential

To assess whether the electrostatic correction preserves the quality of the underlying NequIP potential, we first compared DFT and charge-corrected

Table SI: Energy and force root-mean-square errors of the trained NequIP model on the training and validation sets.

|            | $E_{\text{RMSE}}$ (eV) | $F_{\text{RMSE}}$ (eV/Å) |
|------------|------------------------|--------------------------|
| Training   | 0.00541                | 0.0463                   |
| Validation | 0.00441                | 0.0473                   |

NequIP energies as a function of ionization level for representative clusters. Figures S4 and S5 show the energy difference per atom relative to the compact structures for  $Au_{76}$  and  $Au_{54}$ , respectively, over the charge range  $q = 0-10e$ . In both cases, the charge-corrected NequIP curves closely track the DFT trends: the energies decrease monotonically with increasing charge. The deviations between DFT and the corrected NequIP energies remain small compared to the total stabilization with charge, indicating that the added electrostatic term does not distort the global charge dependence of the PES.

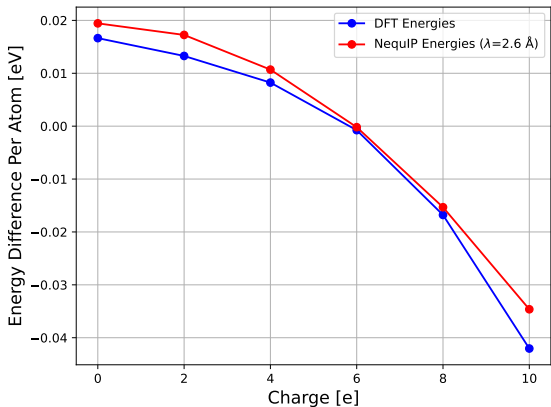


Fig. S4: Energy difference per atom as a function of charge for  $Au_{76}$ , comparing DFT and the charge-corrected NequIP potential. Energies are referenced to the compact structure.

Since the vibrational free energy depends on the curvature of the PES around the minimum, a comparison of vibrational free-energy differences provides an implicit but stringent test of the forces and their

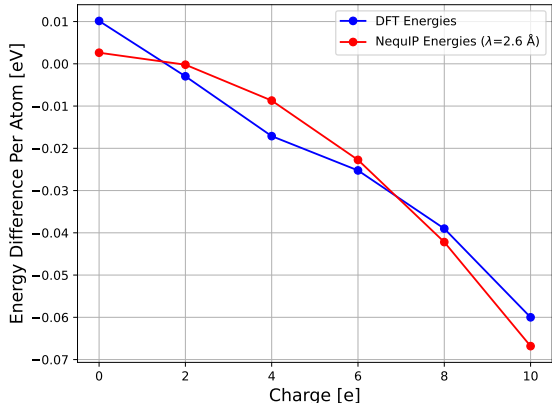


Fig. S5: Energy difference per atom as a function of charge for  $Au_{54}$ , comparing DFT and the charge-corrected NequIP potential. Energies are referenced to the compact structure.

derivatives. Figures S6 and S7 show the vibrational free-energy differences at  $T = 300$  K (including zero-point energy) between planar and compact structures, and between cage and compact structures, respectively. For all considered cluster sizes, the charge-corrected NequIP results closely follow the DFT values: the sign of the free-energy difference is identical in every case, the magnitude is reproduced to good accuracy, and the relative ordering of clusters is preserved. In particular, both DFT and charge-corrected NequIP predict a substantial lowering of the free energy for planar structures relative to compact ones, and a corresponding increase for cage structures relative to their compact counterparts.

Taken together, these comparisons demonstrate that the electrostatic correction preserves both the global charge dependence of the energy and the local curvature around relevant minima. The charge-corrected NequIP potential therefore provides a reliable description of energies and forces for the ionized gold clusters studied here.

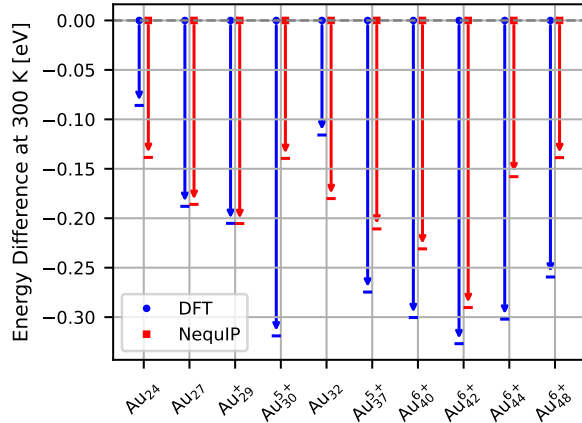


Fig. S6: Vibrational free-energy differences  $\Delta F_{\text{vib}}(300 \text{ K})$  between planar and compact structures for selected clusters, comparing DFT and the charge-corrected NequIP potential. Negative values indicate that the planar structure is favoured at 300K.

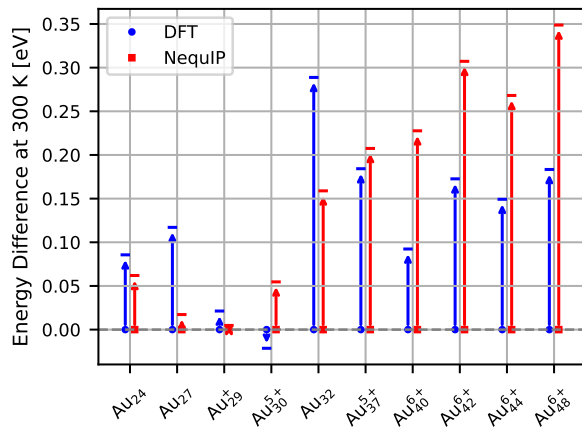


Fig. S7: Vibrational free-energy differences  $\Delta F_{\text{vib}}(300 \text{ K})$  between cage and compact structures for selected clusters, comparing DFT and the charge-corrected NequIP potential. Positive values indicate that the cage structure is higher in free energy than the corresponding compact minimum at 300K.

Table SII: Total energies of the lowest-energy compact, cage and planar structures for the studied gold clusters at the indicated ionization level calculated with PBE XC functional in eV units.

| Size  | Q | $E_{\text{compact}}$ | $E_{\text{cage}}$    | $E_{\text{planar}}$  |
|-------|---|----------------------|----------------------|----------------------|
| Au22  | 0 | -11784373.8829949312 | -11784374.4533069003 | -11784373.6514568999 |
| Au24  | 0 | -12855681.3926772289 | -12855681.7798710000 | -12855681.1892409008 |
| Au26  | 0 | -13926988.7358446382 | -13926988.9359470997 | -13926988.0666028000 |
| Au27  | 0 | -14462642.3687242344 | -14462642.5863713007 | -14462641.4669601992 |
| Au28  | 0 | -14998296.1054223254 | -14998296.3471069001 | -14998294.9480936006 |
| Au29  | 1 | -15533943.9258133303 | -15533944.0681103002 | -15533942.3612922002 |
| Au30  | 0 | -16069603.8613478243 | -16069603.9608851001 | -16069602.0293128993 |
| Au32  | 0 | -17140911.2473042682 | -17140912.4660142921 | -17140909.4174401015 |
| Au34  | 2 | -18212203.5167145170 | -18212203.9256322011 | -18212202.0406000018 |
| Au36  | 4 | -19283485.7045718022 | -19283486.2409333996 | -19283486.1698722988 |
| Au37  | 5 | -19819123.7293879837 | -19819124.1781540997 | -19819124.8460233994 |
| Au38  | 4 | -20354793.7920847908 | -20354794.0276058018 | -20354793.9067832008 |
| Au40  | 4 | -21426101.5680953264 | -21426101.1955628991 | -21426101.5802452005 |
| Au42  | 4 | -22497409.3015969880 | -22497409.6695428044 | -22497408.9425473996 |
| Au44  | 6 | -23568683.3399797492 | -23568683.4833232984 | -23568685.9555942006 |
| Au46  | 6 | -24639991.4168872386 | -24639990.9199844003 | -24639993.8701508008 |
| Au48  | 0 | -25711371.6179627664 | -25711371.7310128994 | -25711368.5723331012 |
| Au50  | 0 | -26782679.0864743069 | -26782679.9584648982 | -26782675.4886697009 |
| Au52  | 2 | -27853972.1115852855 | -27853972.8297604993 | -27853968.8647666983 |
| Au54  | 2 | -28925279.8003975078 | -28925279.9600207992 | -28925276.2220741995 |
| Au55  | 3 | -29460923.1164041013 | -29460923.2176709995 | -29460920.3459875993 |
| Au56  | 6 | -29996531.6094097457 | -29996532.2437016000 | -29996533.6215785000 |
| Au58  | 6 | -31067840.1627144553 | -31067840.5137103982 | -31067841.2947059013 |
| Au60  | 6 | -32139148.0416897386 | -32139148.2349390984 | -32139149.1917935014 |
| Au61  | 7 | -32674783.2398122884 | -32674783.8868740015 | -32674786.2096567005 |
| Au62  | 6 | -33210456.3095684536 | -33210456.6824061610 | -33210456.7862414010 |
| Au64  | 6 | -34281764.5139424354 | -34281764.0594263002 | -34281764.9952920005 |
| Au65  | 7 | -34817399.5628386959 | -34817399.8377309963 | -34817402.4527482986 |
| Au66  | 6 | -35353072.6804527864 | -35353071.9976650029 | -35353072.7357299030 |
| Au68  | 6 | -36424380.4528341815 | -36424379.9037233964 | -36424380.5952892005 |
| Au70  | 8 | -37495649.5527808889 | -37495649.7048689000 | -37495654.6976476000 |
| Au72  | 8 | -38566958.2508317083 | -38566958.1069963000 | -38566962.8893812000 |
| Au74  | 8 | -39638266.3376686349 | -39638266.4942546000 | -39638270.9605859000 |
| Au75  | 7 | -40173939.9928744510 | -40173940.5992190018 | -40173942.0098382011 |
| Au76  | 6 | -40709612.0961799324 | -40709612.1421656013 | -40709611.6766050011 |
| Au78  | 6 | -41780919.9421525151 | -41780920.8910811022 | -41780919.4993818998 |
| Au80  | 6 | -42852228.1418293491 | -42852228.3718110025 | -42852227.1877057031 |
| Au82  | 8 | -43923498.3359515369 | -43923499.8252495974 | -43923502.8322952986 |
| Au84  | 8 | -44994806.2333708853 | -44994807.6258789971 | -44994810.6411446035 |
| Au85  | 7 | -45530480.3363316879 | -45530480.5950400010 | -45530481.2286486998 |
| Au86  | 8 | -46066114.7963887751 | -46066115.5232174993 | -46066118.5422165990 |
| Au88  | 8 | -47137422.8190271556 | -47137423.6060635000 | -47137426.6503728032 |
| Au90  | 8 | -48208731.0783924833 | -48208731.7197723985 | -48208734.2271434963 |
| Au92  | 8 | -49280039.5807077140 | -49280039.7334377989 | -49280042.2704674974 |
| Au94  | 8 | -50351347.5194993913 | -50351347.6239837036 | -50351350.1432097033 |
| Au96  | 8 | -51422655.7879557535 | -51422655.8367601037 | -51422658.0803427994 |
| Au98  | 8 | -52493963.7280049473 | -52493963.7120855972 | -52493965.9882744998 |
| Au100 | 8 | -53565271.7499916703 | -53565272.0851155967 | -53565273.6715193987 |

Table SIII: Total energies of the lowest-energy compact, cage and planar structures for the studied gold clusters at the indicated ionization level calculated with PBEsol+MBD XC functional in eV units.

| Size | Q  | $E_{compact}$        | $E_{cage}$           | $E_{planar}$         |
|------|----|----------------------|----------------------|----------------------|
| Au24 | 7  | -12851992.8814177681 | -12851990.1754461676 | -12851993.9469800312 |
| Au27 | 7  | -14458508.9354776330 | -14458508.0049921852 | -14458510.4501365535 |
| Au29 | 7  | -15529520.1368721183 | -15529520.1599955764 | -15529521.0327065252 |
| Au30 | 7  | -16065025.6610906329 | -16065023.9735914040 | -16065026.2178222984 |
| Au32 | 7  | -17136036.1777288318 | -17136034.2995584235 | -17136036.5220437683 |
| Au37 | 8  | -19813538.1705333702 | -19813535.0545214266 | -19813539.7178942002 |
| Au40 | 8  | -21420053.9577834904 | -21420051.9037468024 | -21420055.4860454276 |
| Au42 | 9  | -22491039.1179469712 | -22491036.8775570393 | -22491042.5188986212 |
| Au44 | 9  | -23562049.4228905290 | -23562048.0477586761 | -23562053.2435088828 |
| Au48 | 9  | -25704071.2119783461 | -25704068.2209315747 | -25704073.6852728166 |
| Au50 | 9  | -26775082.5192736201 | -26775077.9584287070 | -26775084.2105447613 |
| Au52 | 9  | -27846094.1124891043 | -27846089.1916963086 | -27846094.3166619316 |
| Au55 | 10 | -29452584.0350670293 | -29452579.2255310230 | -29452586.7437124103 |
| Au56 | 10 | -29988089.1973293573 | -29988084.0762551837 | -29988091.9731848203 |
| Au60 | 10 | -32130109.3035199046 | -32130105.5282131210 | -32130112.4390639514 |
| Au61 | 10 | -32665614.8136003278 | -32665610.5654794015 | -32665617.1123959087 |
| Au62 | 10 | -33201118.7035499662 | -33201116.9057762623 | -33201122.2153994143 |
| Au64 | 10 | -34272131.2917612493 | -34272126.0756461248 | -34272133.0516912043 |
| Au65 | 10 | -34807635.6655190289 | -34807631.3757642657 | -34807637.7224883810 |
| Au68 | 10 | -36414152.3406183347 | -36414146.5469158441 | -36414153.4039350450 |
| Au70 | 10 | -37485163.1232914180 | -37485156.5913205147 | -37485163.2896568999 |
| Au75 | 11 | -40162662.4295440763 | -40162656.7347052917 | -40162665.5549834371 |
| Au76 | 11 | -40698167.5411698073 | -40698162.3049923852 | -40698171.0495504960 |
| Au78 | 11 | -41769177.6778317764 | -41769172.5451158136 | -41769180.3056200817 |
| Au80 | 11 | -42840189.5489087030 | -42840183.2280374393 | -42840190.5364795625 |
| Au85 | 12 | -45517688.6020401269 | -45517682.9921225086 | -45517692.8950748593 |

Table SIV: Total energies of the lowest-energy compact, cage and planar structures for the studied gold clusters at the indicated ionization level calculated with r<sup>2</sup>SCAN functional in eV units.

| Size | Q | $E_{\text{compact}}$ | $E_{\text{cage}}$    | $E_{\text{planar}}$  |
|------|---|----------------------|----------------------|----------------------|
| Au24 | 0 | -12855515.9595729932 | -12855516.6123223491 | -12855515.2829093002 |
| Au27 | 0 | -14462456.7595318630 | -14462456.9645614643 | -14462454.9352743775 |
| Au29 | 1 | -15533744.6757797468 | -15533744.7820909619 | -15533742.0970994346 |
| Au30 | 5 | -16069338.7766732369 | -16069338.9568433017 | -16069339.7718810383 |
| Au32 | 0 | -17140691.7607096955 | -17140692.5649791211 | -17140688.5184396170 |
| Au37 | 5 | -19818869.7899332419 | -19818870.0673865154 | -19818869.7279463746 |
| Au40 | 6 | -21425792.6897237673 | -21425792.2200301364 | -21425794.1400935724 |
| Au42 | 6 | -22497087.4161620438 | -22497086.8574161083 | -22497088.2642474622 |
| Au44 | 6 | -23568382.1040482968 | -23568381.4029078223 | -23568382.6969524436 |
| Au48 | 6 | -25710971.3836712800 | -25710969.9138409160 | -25710971.3817078769 |
| Au50 | 7 | -26782245.8384333365 | -26782244.5643433854 | -26782247.7779425494 |
| Au52 | 6 | -27853559.4697657786 | -27853559.1002398059 | -27853560.1268005781 |
| Au55 | 6 | -29460501.4421241246 | -29460501.4501994476 | -29460501.1217344627 |
| Au56 | 7 | -29996129.1721618697 | -29996128.8554048650 | -29996130.8869261593 |
| Au60 | 7 | -32138718.5432152487 | -32138717.9837394021 | -32138719.3619752303 |
| Au61 | 8 | -32674344.6072562374 | -32674344.6977852881 | -32674347.6937589720 |
| Au62 | 8 | -33209992.2565247416 | -33209992.3066731915 | -33209994.8916107081 |
| Au64 | 8 | -34281287.5649208203 | -34281286.2623199895 | -34281290.0366618708 |
| Au65 | 8 | -34816934.5829489604 | -34816933.6845940202 | -34816936.9615447745 |
| Au68 | 8 | -36423877.1656726077 | -36423875.2970955744 | -36423879.0072333813 |
| Au70 | 8 | -37495171.4333114251 | -37495169.5787350461 | -37495173.0350215882 |
| Au75 | 8 | -40173407.8779937848 | -40173406.6102867797 | -40173408.8073367774 |
| Au76 | 8 | -40709055.1760824099 | -40709053.9038519040 | -40709056.1566343531 |
| Au78 | 8 | -41780349.7217550129 | -41780348.7655952126 | -41780350.2157986462 |
| Au80 | 8 | -42851644.5419136807 | -42851643.8219444156 | -42851644.8369588703 |
| Au85 | 9 | -45529859.4852932543 | -45529858.6832017750 | -45529862.1163276657 |

## References

- 1 Peter E. Blöchl. Projector augmented-wave method. *Phys. Rev. B*, 50:17953–17979, 1994. doi: 10.1103/PhysRevB.50.17953.
- 2 Georg Kresse and Daniel Joubert. From ultrasoft pseudopotentials to the projector augmented-wave method. *Phys. Rev. B*, 59:1758–1775, 1999. doi: 10.1103/PhysRevB.59.1758.
- 3 Georg Kresse and Jürgen Furthmüller. Efficient iterative schemes for ab initio total-energy calculations using a plane-wave basis set. *Phys. Rev. B*, 54:11169–11186, 1996. doi: 10.1103/PhysRevB.54.11169.
- 4 Georg Kresse and Jürgen Furthmüller. Efficiency of ab-initio total energy calculations for metals and semiconductors using a plane-wave basis set. *Comput. Mater. Sci.*, 6:15–50, 1996. doi: 10.1016/0927-0256(96)00008-0.
- 5 John P. Perdew, Kieron Burke, and Matthias Ernzerhof. Generalized gradient approximation made simple. *Phys. Rev. Lett.*, 77:3865–3868, 1996. doi: 10.1103/PhysRevLett.77.3865.
- 6 Murray S. Daw and M. I. Baskes. Embedded-atom method: Derivation and application to impurities, surfaces, and other defects in metals. *Phys. Rev. B*, 29:6443–6453, 1984. doi: 10.1103/PhysRevB.29.6443.
- 7 C. J. O’Brien, C. M. Barr, P. M. Price, K. Hattar, and S. M. Foiles. Grain boundary phase transformations in ptau and relevance to thermal stabilization of bulk nanocrystalline metals. *J. Mater. Sci.*, 53:2911–2927, 2018. doi: 10.1007/s10853-017-1706-1.
- 8 Raju P. Gupta. Lattice relaxation at a metal surface. *Phys. Rev. B*, 23:6265–6270, 1981. doi: 10.1103/PhysRevB.23.6265.